

XAS characterization and CO oxidation on zirconia-supported LaFeO₃ perovskite

S. Colonna^a, S. De Rossi^b, M. Faticanti^b, I. Pettiti^{b,*}, P. Porta^b

^a *Istituto di Struttura della Materia, CNR, Via Fosso del Cavaliere 100, 00133 Rome, Italy*

^b *Dipartimento di Chimica, Istituto IMIP (ex centro di Studio su "ruttura ed Attività Catalitica di Sistemi di Ossidi" SACS), Università degli Studi di Roma, CNR, Sapienza Piazzale Aldo Moro 5, 00185 Rome, Italy*

Received 6 February 2002; accepted 23 April 2002

Abstract

ZrO₂-supported La, Fe containing catalysts were prepared by impregnation of tetragonal ZrO₂ with citrate-type precursors and calcination at 1073 K. The catalysts were characterized by X-ray diffraction (XRD), X-ray absorption spectroscopy (XAS) and BET specific surface area (SA) determination. The catalytic activity towards CO oxidation was tested in the range 400–900 K. XRD revealed the presence of tetragonal zirconia with traces of the monoclinic phase. LaFeO₃ perovskite was detected for La, Fe loading higher than 6%. XAS suggested that LaFeO₃ was formed at lower loading too. The catalytic investigation evidenced that the presence of Fe is necessary for making highly active catalysts, whose performance improves with increasing the iron content.

© 2002 Elsevier Science B.V. All rights reserved.

Keywords: Zirconia-supported La–Fe perovskite; XAS; Catalytic CO oxidation

1. Introduction

Most of the catalysts used in modern industrial applications is based on mixed metal oxides. Among these, perovskite-type oxides represent a prominent and very studied class of materials [1,2]. The perovskite oxides have general formula ABO₃ in which A is the larger cation and B the smaller one. The ideal perovskite-type structure is cubic with the A cation at the center of the cube 12-fold coordinated with oxygen anions and the B cations occupying the corners of the cube in a six-fold coordination. Deviations from the ideality with orthorhombic (e.g. LaFeO₃) or rhombohedral (e.g. LaMnO₃ and LaCoO₃) symmetry are also known. The great va-

riety of properties that these compounds exhibit is due to the fact that around 90% of the metallic elements in the periodic table can give stable perovskite-type structures and also multicomponent perovskites by partial substitution of cations in A and/or B position. The only rule to be needed in order to form a perovskite-type structure is a ionic radii requirement introduced by Goldschmidt [3], the so called tolerance factor (t) defined by the equation $t = (r_A + r_O) / \sqrt{2}(r_B + r_O)$, where $0.75 < t < 1.0$ and r_A , r_B and r_O are the ionic radii of the cations A and B and of the oxygen anions, respectively. The possibility of including several metal cations into the structure accounts for the large variety of reactions in which perovskites are used as catalysts, for instance, total oxidation of hydrocarbons, CO oxidation, NO_x decomposition, hydrogenation and hydrogenolysis reactions and so on. Moreover,

* Corresponding author. Fax: +39-06-490324.
E-mail address: ida.pettiti@uniroma1.it (I. Pettiti).

these oxides can be excellent materials not only for catalytic investigations but also for establishing correlations between reactivity and surface and/or bulk properties.

The preparation of perovskite-type oxides is a very important task, particularly if the goal is to obtain high surface area (SA) materials good for catalytic purposes. A method based on citrate precursors was used [4] which allows to obtain perovskites with a few tens $\text{m}^2 \text{g}^{-1}$ of specific SA after calcination at 1073 K. In our laboratory many perovskite-type oxides have been already synthesized, characterized for their solid state properties and catalytically tested for methane and CO oxidation [5–11] and for methane coupling [12]. Moreover, the dispersion of an active phase on a suitable support is the most common and convenient way to increase the possibility of contacting the active material and the reactant species. Therefore, a project started in our laboratory in order to investigate the structural and catalytic properties of materials prepared by impregnating a support with proper precursors and submitting this system to the same thermal treatments used to prepare the bulk perovskite. Some supported perovskite phases have already been reported in the literature [13–18]. In our investigation the precursors were always citrate-type and tetragonal zirconia was the first support to be prepared and used. The zirconia support should represent a good choice thanks to its high SA and moderate interactions with perovskite. Previous investigations on ZrO_2 -supported La–Mn [19] and La–Co [20] materials revealed that in both systems perovskite was formed at a loading higher than 6%. In addition, the La–Mn/ ZrO_2 samples showed the formation of disordered La and Mn oxide species at low loading, while the La–Co/ ZrO_2 samples showed the formation of disordered La–Co mixed oxide species at low loading, and of Co_3O_4 at high loading.

In order to carry on and broaden the research in the field of supported perovskites, the present study reports the main results concerning the preparation, XRD and XAS characterization and catalytic investigation towards CO oxidation of zirconia supported La–Fe samples with different metals loading (hereafter, labeled ZLaFe– x where x stands for the wt.% of loading of the supported species assumed as LaFeO_3 perovskite in the calculation).

2. Experimental

ZLaFe supported catalysts with different La–Fe loading (2, 4, 6, 12 and 16 wt.%) were prepared by impregnation of tetragonal ZrO_2 with the appropriate amount of citrate precursors.

Tetragonal ZrO_2 with a large SA was prepared by the method of Chuah et al. [21]. An aqueous solution of ZrOCl_2 0.075 M was added, dropwise (1 ml min^{-1}) and under magnetic stirring, to a 5 M NH_4OH solution. The hydrous zirconia, after digestion in its mother solution at 373 K for 48 h, was filtered, washed with water until the AgNO_3 test gave no opalescence in the washing solution, then dried in a furnace overnight at 383 K and finally calcined at 1073 K for 5 h (raising slowly the temperature by 1 K min^{-1}).

The dispersion of LaFeO_3 on the ZrO_2 support was performed by the citrate method [4,14]. Two solutions were added to a weighted amount of ZrO_2 , an aqueous solution of citric acid was added first and subsequently a solution containing $\text{La}(\text{NO}_3)_3$ and $\text{Fe}(\text{NO}_3)_3$ in equimolar proportions. The molar ratio between the citric acid and the overall metal nitrates was fixed at 1. The resulting solution was kept at 383 K until dryness and the samples, after grinding, were calcined at 1073 K for 5 h. For a comparison between catalytic activities, two samples containing respectively La and Fe with a 6 wt.% loading (labeled ZLa–6 and ZFe–6) were also prepared. For a phase check, unsupported LaFeO_3 was prepared by the citrate method [4,22].

Phase analysis was performed by XRD using a Philips PW 1029 diffractometer with Ni-filtered $\text{Cu K}\alpha$ radiation and equipped with a computer for data acquisition and analysis (software APD-Philips).

BET SA of the samples (SA, $\text{m}^2 \text{g}^{-1}$) was evaluated by nitrogen adsorption at 77 K in a vacuum glass apparatus.

XAS measurements at the Fe K-edge were performed for the ZLaFe–2, –6 and –12 supported samples, and for LaFeO_3 and $\alpha\text{-Fe}_2\text{O}_3$ as reference materials. These measurements were collected at the beamline GILDA, ESRF, Grenoble (France) in fluorescence detection mode for the catalyst samples and in transmission mode for the reference compounds. The beamline monochromator was equipped with two Si (311) crystals. Powder samples were deposited on Millipore membranes or mixed to an appropriate amount of boron nitride (BN) and pressed into pellets.

During the data collection samples were held at the liquid nitrogen temperature. The XANES part of the experimental signal was obtained by subtracting a linear pre-edge and normalizing to one in correspondence of the first EXAFS oscillation. The EXAFS analysis was performed by using the complete FEFF8 package [23]. Fourier transforms (FTs) for the signal $k^3\chi(k)$ were calculated in the range $2.7 < k < 11.5 \text{ \AA}^{-1}$ by using a Kaiser window. Structural information was obtained by fitting the $FT(R)$ function in the 1.0–4.0 \AA range.

The CO oxidation with O_2 was studied in a flow system in the range 400–900 K using 0.5 g of catalyst supported on a silica fritted disk internal to a silica reactor vertically positioned in a tubular electrical heater. A Ni–NiCr thermocouple was positioned in the middle of the catalyst bed. An ASCON XS proportional programmer powered the heater and was set to produce a linear temperature ramp of 1 K min^{-1} in the experimental range. The composition and the total flow rate of the reactants was adjusted to 1% CO, 20% O_2 , balance He by volume and $100 \text{ cm}^3 \text{ STP min}^{-1}$, employing independent electronic mass flow controllers MKS model 1259 driven by a MKS unit model 147. The space velocity resulted $12\,000 \text{ cm}^3 \text{ STP h}^{-1} \text{ g}^{-1}$. At time intervals of 20 min, that is every 20 K, a sample of 1 cm^3 of effluent from the reactor was sampled and analyzed by gas-chromatography, using an Alltech CTR 1 column made of two coaxial columns held at RT. The inner column was packed with Porapak[®], whereas the outer one contained a molecular sieve packing. A thermal conductivity detector was used to reveal CO_2 , O_2 and residual CO. The mass balance with respect to carbon was $100 \pm 2\%$. Before each run a standard pretreatment at 773 K with oxygen in flow at $100 \text{ cm}^3 \text{ STP min}^{-1}$ and 0.5 h was carried out. For some catalysts the run was repeated after the oxygen treatment and the conversion values were reproduced to within $\pm 3\%$ in the whole range of reaction temperatures.

3. Results and discussion

3.1. Structural properties

Phase analysis, performed by X-ray diffraction, showed that up to 6% loading no other phase but tetragonal zirconia (with traces of the monoclinic

phase) was revealed. Fig. 1 shows the XRD patterns for all the ZLaFe supported samples and LaFeO_3 unsupported perovskite; asterisks indicate the peaks that are related to the perovskite phase. Patterns for the ZLa–6 and ZFe–6 samples (not reported in the figure) show only peaks related to the zirconia support. In Table 1 the phases detected by XRD are reported.

For all the ZLaFe samples the SA values are in the range $47\text{--}85 \text{ m}^2 \text{ g}^{-1}$. The SA values for ZLa–6 and ZFe–6 samples are 45 and $32 \text{ m}^2 \text{ g}^{-1}$, respectively. The ZrO_2 support and the LaFeO_3 and $\alpha\text{-Fe}_2\text{O}_3$ reference compounds show SA values equal to 83, 6 and $2 \text{ m}^2 \text{ g}^{-1}$, respectively. All the SA values are reported in Table 1.

The structural investigation of the ZLaFe–2, –6 and –12 samples was undertaken by XAS spectroscopy at the Fe K-edge. The high local sensitivity of this technique allows to better evidence structural characteristics of the supported phases and to make a comparison between samples with low and high metals loading.

First derivatives of the XANES spectra are reported in Fig. 2. The supported ZLaFe samples show a maximum at 7126 eV resembling that of pure LaFeO_3 perovskite. A broadening of this maximum towards lower energy values is also visible and could be attributed to a small and dispersed amount of ferric oxide present on the zirconia surface together with a perovskite-like phase.

This hypothesis was confirmed by the EXAFS analysis. Fig. 3 shows the Fourier transforms (solid lines) of the EXAFS signals for the ZLaFe samples compared to pure LaFeO_3 and $\alpha\text{-Fe}_2\text{O}_3$. In the same figure the dashed lines represent the fits obtained by using the standard EXAFS formula. For the ZLaFe samples, FTs reveal intense and well defined first shell features in the 0.8–2.0 \AA range, due to oxygen nearest neighbors, while peaks related to following coordination shells are not so evident. The first shell features of the samples appear in the same position as those shown in the FT of pure LaFeO_3 . In fact, for both the LaFeO_3 and $\alpha\text{-Fe}_2\text{O}_3$ reference compounds the first shell peaks are visible in the same 0.8–2.0 \AA range, but for $\alpha\text{-Fe}_2\text{O}_3$ these peaks are shifted to lower R values as compared with LaFeO_3 (and with ZLaFe samples too). In a previous work by Okamoto et al. [24], ZrO_2 -supported Fe oxide catalysts, with an iron loading ranging from 1 to 10 wt.%, were investigated

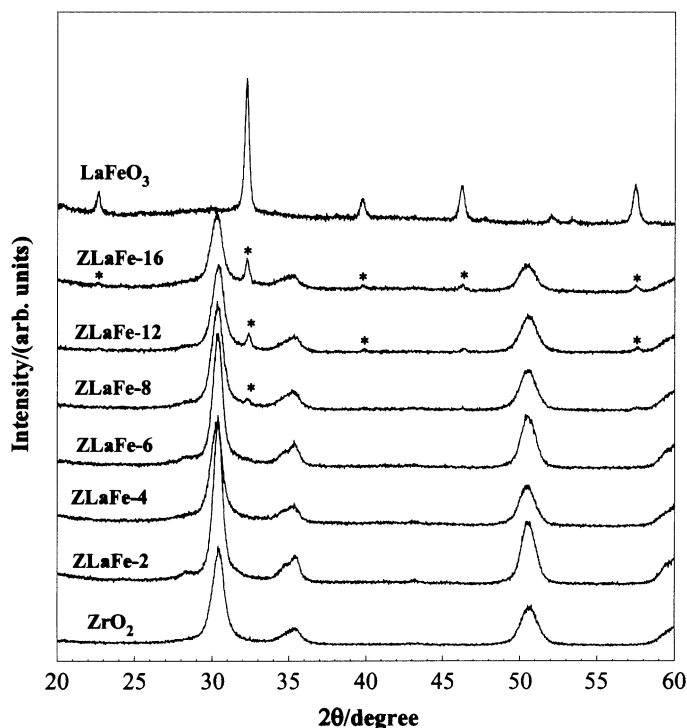


Fig. 1. XRD patterns of ZrO_2 , $LaFeO_3$ and ZLaFe samples. Asterisks indicate the most intense X-ray lines of $LaFeO_3$.

by EXAFS spectroscopy revealing FTs very similar in shape and peaks position to the FT of $\alpha-Fe_2O_3$. This evidence can be a further confirmation that something different from $\alpha-Fe_2O_3$ has been formed on the surface of the zirconia support in our ZLaFe samples.

The FTs of the $LaFeO_3$ and $\alpha-Fe_2O_3$ reference compounds were fitted by using the main crystallographic bond distances data [25,26], and leaving free the E_0 shift, the S_0^2 term and the Debye–Waller factors. In the fitting procedure of the ZLaFe samples two

Table 1
Samples, XRD phases, SA and kinetic parameters for CO oxidation

Catalyst	XRD phases	mol_{Fe} $g^{-1} \times 10^3$	SA ($m^2 g^{-1}$)	E_a ($kJ mol^{-1}$)	Kinetic constant (first-order with respect to CO) at 573 K		
					k_W (mol_{CO_2} $h^{-1} g^{-1} \times 10^2$)	k_S (mol_{CO_2} $h^{-1} m^{-2} \times 10^4$)	k_{Fe} (mol_{CO_2} $h^{-1} mol_{Fe}^{-1}$)
ZrO_2	ZrO_2T	–	83	80	0.07	0.08	–
ZLaFe–2	ZrO_2T	0.082	53	29	0.19	0.37	24
ZLaFe–4	ZrO_2T	0.165	85	39	0.34	0.40	21
ZLaFe–6	ZrO_2T	0.247	63	52	0.36	0.57	15
ZLaFe–8	$ZrO_2T + LaFeO_3$	0.330	63	68	0.41	0.65	12
ZLaFe–12	$ZrO_2T + LaFeO_3$	0.494	79	46	0.74	0.93	15
ZLaFe–16	$ZrO_2T + LaFeO_3$	0.659	47	51	0.47	0.99	7.1
ZFe–6	ZrO_2T	1.08	32	79	0.08	0.26	0.8
ZLa–6	ZrO_2T	–	45	42	0.04	0.08	–
$LaFeO_3$	$LaFeO_3$	4.12	6	80	0.15	2.5	0.4
$\alpha-Fe_2O_3$	$\alpha-Fe_2O_3$	12.5	2	90	2.7	134	2.1

ZrO_2T : tetragonal zirconia.

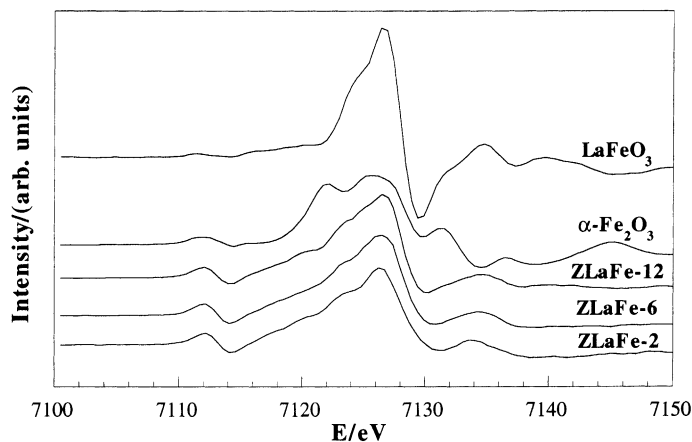


Fig. 2. First derivatives of XANES spectra for the ZLaFe samples compared to LaFeO₃ and α -Fe₂O₃ reference compounds.

Fe–O contributions were used to reproduce the first near neighbors coordination. The second shell structures were fitted by using both Fe–La and Fe–Fe contributions. Debye–Waller, E_0 and S_0^2 parameters were fixed to the value obtained from the fit of the reference compounds. The coordination numbers (N) and

bond distances (R) were left to vary in the fit. The Debye–Waller factors were fixed to avoid the strong correlation with the coordination numbers. The fit results, reported in Table 2, reveal that in the three samples the distances related to the Fe–O and Fe–La bond length are very similar to those of LaFeO₃ perovskite.

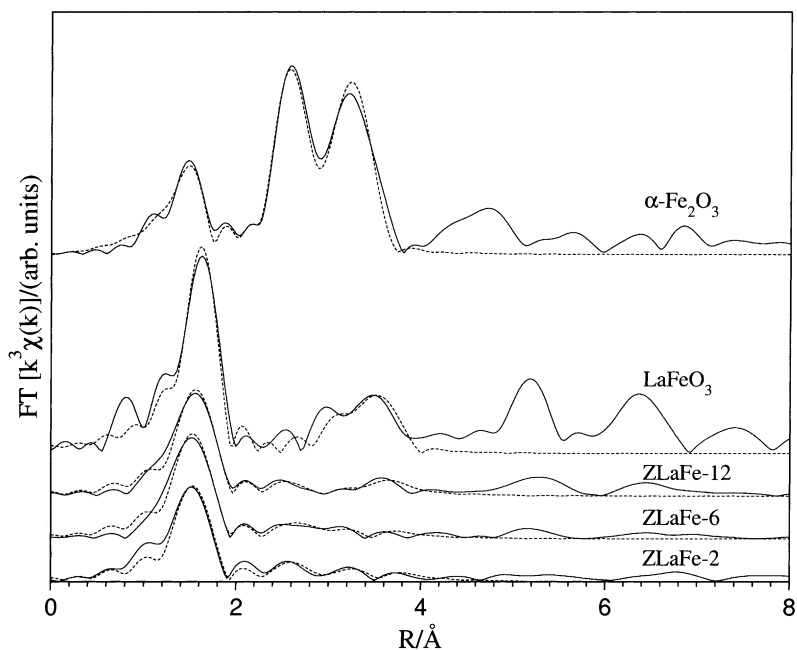


Fig. 3. Fe K-edge: Fourier transforms of the $k^3\chi(k)$ signals for the ZLaFe–2, –6 and –12 samples compared to pure LaMnO₃ and α -Fe₂O₃. The continuous line represents the experimental data and the dots are the fit profiles.

Table 2

Coordination numbers (N) and bond distances (R) obtained from EXAFS data for ZLaFe, LaFeO₃ and α -Fe₂O₃ samples

FeK-edge shell	Fe–O	Fe–O	Fe–La	Fe–La	Fe–Fe	Fe–Fe					
ZLaFe–2											
$N \pm 0.3$	2.3	0.9	1.9	2.9	2.8	0.5					
$R (\text{\AA}) \pm 0.02$	1.96	2.11	3.32	3.76	3.83	3.02					
ZLaFe–6											
$N \pm 0.3$	2.5	1.3	2.6	3.39	3.2	0.5					
$R (\text{\AA}) \pm 0.02$	1.96	2.09	3.28	3.71	3.78	3.03					
ZLaFe–12											
$N \pm 0.3$	2.4	1.3	3.9	4.7	4.2	0.4					
$R (\text{\AA}) \pm 0.02$	1.97	2.09	3.32	3.80	3.83	3.06					
LaFeO ₃											
N	4.0	2.0	4.0	4.0	6.0	–					
$R (\text{\AA})$	1.99	2.10	3.35	3.76	3.93	–					
α -Fe ₂ O ₃ shells	Fe–O	Fe–O	Fe–Fe	Fe–Fe	Fe–Fe	Fe–O	Fe–O	Fe–Fe	Fe–O	Fe–Fe	
N	3.0	3.0	1.0	3.0	3.0	3.0	3.0	6.0	3.0	1.0	
$R (\text{\AA})$	1.95	2.11	2.89	2.97	3.37	3.40	3.60	3.70	3.78	3.99	

The coordination numbers are smaller than those expected, probably owing to a very disordered distribution of perovskite-like species on the zirconia surface and/or to the presence of small crystallites. However, the coordination numbers increase with increasing the La and Fe content, indicating a greater degree of particles aggregation at higher loading.

As to the Fe–Fe bond lengths, the ZLaFe samples show a distance at about 3.80 Å that is slightly shorter than that of pure LaFeO₃ (3.93 Å). Moreover, the fits improved remarkably by adding a further Fe–Fe contribution which resulted to be a short bond distance (about 3.03 Å) with very small coordination numbers ($N = 0.4$ – 0.5). Such a contribution could suggest the presence of a small amount of very dispersed α -Fe₂O₃ which exhibits short Fe–Fe bond distances at 2.97 and 3.37 Å, respectively, and a longer one at 3.70 Å. The simultaneous presence of different phases, mainly perovskite and some ferric oxide, very disordered and dispersed on the zirconia surface, should be confirmed also considering that the 3.70 Å Fe–Fe distance, belonging to α -Fe₂O₃, could affect the values of the longer distances found in the ZLaFe samples. These bond lengths resulted to be shorter than 3.93 Å, that is the value of Fe–Fe bond distance in LaFeO₃. Therefore, the fitted distances, found in the ZLaFe supported samples, resulted to be intermediate values between the Fe–Fe bond distances in the two oxidic phases.

3.2. Catalytic properties

The activity of zirconia support was measurable starting from 570 K and the CO conversion was 70% at 800 K (Fig. 4). Similar conversion values were shown by the catalyst ZLa–6, pointing to a low activity of both zirconium and lanthanum oxide species.

Concerning the iron containing catalysts, they were substantially more active in comparison with ZrO₂ and ZLa–6. The transition metal is therefore essential for developing high activity. Most probably this is so because of the ease of surface local change of the iron oxidation state with ensuing improvement of the redox steps of the reaction. Except the more dilute Fe containing catalyst, ZLaFe–2, that reaches 83% conversion at 800 K, the iron based catalysts reached 100% conversion below 800 K, the α -Fe₂O₃ sample showing 100% conversion at 580 K already.

The conversion level trends with the reaction temperature, shown in Fig. 4, clearly indicates a quite large range of apparent activation energy, E_a , values for the different samples. Quantification of E_a was obtained from Arrhenius plots (not shown) in which the kinetic constants (first-order with respect to CO and pseudo zeroth-order with respect to oxygen, present in large excess) were reported versus the reciprocal of temperature (K). The kinetic constants were evaluated in the range from some percentage to about 80% conversion.

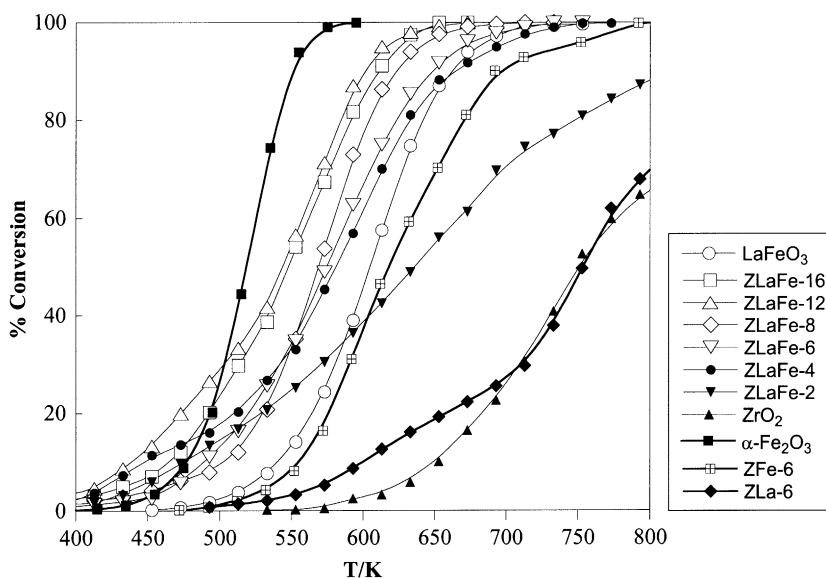


Fig. 4. CO conversion as a function of the reaction temperature.

Table 1 reports the E_a data and the kinetic constants per gram of catalyst (k_W), per unit surface area (k_S) and per mol of iron (k_{Fe}), evaluated from the Arrhenius plots at the reaction temperature of 573 K (in few cases extrapolation was necessary).

Based on k_S (Table 1), among the pure compounds, the order of activity is $\alpha\text{-Fe}_2\text{O}_3 \gg \text{LaFeO}_3 \gg \text{ZrO}_2$. This is true in all the temperature range, being the apparent activation energies of the samples rather close (90, 80, 80 KJ mol^{-1} , respectively). Concerning the ZLaFe supported samples, they show E_a values lower than those of the pure compounds suggesting that the structure of the active site and/or the enthalpy of the CO adsorption change with composition in a complex way. Table 1 shows that the k_S values of the ZLaFe samples are similar, however showing a definite increase with iron content from 2 to 16%. A parallel decrease in the k_{Fe} values at the increase of the iron content for ZLaFe catalysts is consistent with a higher dispersion of the active material at lower loading.

4. Conclusions

XRD analysis for the La–Fe zirconia supported samples shows only the tetragonal zirconia phase with

traces of monoclinic zirconia. At higher loading XRD also shows the presence of the perovskite LaFeO_3 phase.

XAS analysis, performed for the ZLaFe–2, –6 and –12 materials, reveals the formation of LaFeO_3 dispersed on zirconia also at a loading lower than 6%. In addition to perovskite, a small amount of very dispersed $\alpha\text{-Fe}_2\text{O}_3$ should be formed.

As to the catalytic performance, pure zirconia and ZLa–6 display very low activity in CO oxidation. ZLaFe–2 is substantially more active so pointing to Fe as essential for high catalytic activity. $\alpha\text{-Fe}_2\text{O}_3$ is by far the more active catalyst even in comparison with LaFeO_3 . ZLaFe catalysts display catalytic activity increasing with the iron content and, as expected, activity data suggest higher surface dispersion at lower loading.

References

- [1] L.G. Tejuca, J.L.G. Fierro (Eds.), Properties and Applications of Perovskite-type Oxides, Marcel Dekker, New York, 1993.
- [2] M.A. Peña, J.L.G. Fierro, Chem. Rev. 101 (2001) 1981.
- [3] V.M. Godschmidt, Skr. Nor. Viedensk.-Akad., Kl. Part I. Mater.-Naturvidensk. Kl, no. 8, 1926.
- [4] (a) Belgium Patent 735, 476 (1969);
(b) B. Delmon, J. Droguest, Fine particles, in: W.H. Fuhn

- (Ed.), Proceedings of the Second International Conference, The Electrochemical Society, p. 242.
- [5] L. Lisi, G. Bagnasco, P. Ciambelli, S. De Rossi, P. Porta, G. Russo, M. Turco, J. Solid State Chem. 146 (1999) 176.
- [6] P. Porta, S. De Rossi, M. Faticanti, G. Minelli, I. Pettiti, M. Turco, J. Solid State Chem. 146 (1999) 291.
- [7] P. Ciambelli, S. Cimino, S. De Rossi, M. Faticanti, L. Lisi, G. Minelli, I. Pettiti, P. Porta, G. Russo, M. Turco, Appl. Catal. B: Environ. 24 (2000) 243.
- [8] P. Ciambelli, S. Cimino, S. De Rossi, L. Lisi, G. Minelli, P. Porta, G. Russo, Appl. Catal. B: Environ. 29 (2001) 239.
- [9] P. Porta, S. Cimino, S. De Rossi, M. Faticanti, G. Minelli, I. Pettiti, Mater. Chem. Phys. 71 (2001) 165.
- [10] P. Ciambelli, S. Cimino, M. Faticanti, L. Lisi, G. Minelli, I. Pettiti, P. Porta, Appl. Catal. B: Environ. 33 (2001) 193.
- [11] R. Spinicci, A. Tofanari, M. Faticanti, I. Pettiti, P. Porta, J. Mol. Catal. A: Chem. 176 (2001) 247.
- [12] R. Spinicci, P. Marini, S. De Rossi, M. Faticanti, P. Porta, J. Mol. Catal. A: Chem. 176 (2001) 253.
- [13] H. Fujii, N. Mizuno, M. Misono, Chem. Lett., 1987, 2147.
- [14] H.M. Zhang, Y. Teraoka, N. Yamazoe, Appl. Catal. 41 (1988) 137.
- [15] A.K. Ladavos, P.J. Pomonis, Appl. Catal. B: Environ. 2 (1993) 27.
- [16] S.D. Peter, E. Garbowsky, V. Perrichon, B. Pommier, M. Primet, Appl. Catal. A: Gen. 205 (2001) 147.
- [17] N. Mizuno, H. Fujii, H. Igarashi, M. Misono, J. Am. Chem. Soc. 114 (1992) 7151.
- [18] K. Stephan, M. Hackenberger, D. Kiessling, G. Wendt, Catal. Today 54 (1999) 23.
- [19] S. Cimino, S. Colonna, S. De Rossi, M. Faticanti, L. Lisi, I. Pettiti, P. Porta, J. Catal. 205 (2002) 309.
- [20] S. Colonna, S. De Rossi, M. Faticanti, I. Pettiti, P. Porta, J. Mol. Catal. A: Chem. 180 (2002) 161.
- [21] G.K. Chuah, S. Janice, S.A. Cheong, K.S. Chan, Appl. Catal. A: Gen. 145 (1996) 267.
- [22] H.M. Zhang, Y. Teraoka, N. Yamazoe, Chem. Lett., 1987, p. 665.
- [23] A.L. Ankudinov, B. Ravel, J.J. Rehr, S.D. Conradson, Phys. Rev. B 58 (1998) 7565.
- [24] Y. Okamoto, T. Kubota, Y. Ohto, S. Nasu, J. Catal. 192 (2000) 412.
- [25] S. Geller, E.A. Wood, Acta Cryst. 9 (1956) 563.
- [26] R.W.G. Wyckoff, Crystal Structures, 2nd Edition, Vol. 2, Wiley, New York, 1964, p. 6.